

Structural evolution of fault zones in sandstone by multiple deformation mechanisms: Moab fault, southeast Utah

Nicholas C. Davatzes[†]

Peter Eichhubl[‡]

Atilla Aydin

Department of Geological and Environmental Science, Stanford University, Stanford, California 94305-2115, USA

ABSTRACT

Faults in sandstone are frequently composed of two classes of structures: (1) deformation bands and (2) joints and sheared joints. Whereas the former structures are associated with cataclastic deformation, the latter ones represent brittle fracturing, fragmentation, and brecciation. We investigated the distribution of these structures, their formation, and the underlying mechanical controls for their occurrence along the Moab normal fault in southeastern Utah through the use of structural mapping and numerical elastic boundary element modeling. We found that deformation bands occur everywhere along the fault, but with increased density in contractional relays. Joints and sheared joints only occur at intersections and extensional relays. In all locations, joints consistently overprint deformation bands. Localization of joints and sheared joints in extensional relays suggests that their distribution is controlled by local variations in stress state that are due to mechanical interaction between the fault segments. This interpretation is consistent with elastic boundary element models that predict a local reduction in mean stress and least compressive principal stress at intersections and extensional relays. The transition from deformation band to joint formation along these sections of the fault system likely resulted from the combined effects of changes in remote tectonic loading, burial depth, fluid pressure, and rock properties. In the case of the Moab

fault, we conclude that the structural heterogeneity in the fault zone is systematically related to the geometric evolution of the fault, the local state of stress associated with fault slip, and the remote loading history. Because the type and distribution of structures affect fault permeability and strength, our results predict systematic variations in these parameters with fault evolution.

Keywords: deformation band, joint, Moab fault, mechanics, stress, sheared joint.

INTRODUCTION

Brittle faults are complex zones of localized shear that are composed of smaller, fundamental, structures. It is the type, distribution, and arrangement of these fundamental structures that control the mechanical and hydrologic properties of the fault zone (Aydin, 1978; McGrath and Davison, 1995; Caine et al., 1996; Willemsse et al., 1997; Foxford et al., 1998; Vermilye and Scholz, 1998; Schulz and Evans, 2000; Aydin, 2000; Jourde et al., 2002). Because of this structural complexity, conceptual models of fault formation that attempt to predict these properties are largely heuristic rather than process based. Predictive process-based models of faulting require that the mechanics of fault growth, and the formation of these fundamental structures, are reasonably well understood.

It has been recognized that faults evolve by adding new structures as slip accumulates (Cartwright et al., 1995; Cowie, 1998; Shipton and Cowie, 2001, 2003; Davatzes et al., 2003; Crider and Peacock, 2004; Kim et al., 2004). These studies have shown that new structures develop at the tip of the fault in association with fault growth, as well as in rock adjacent to the fault or within the fault zone. In sandstone, faults are frequently composed of two classes of structures (Davatzes and Aydin, 2003): (1) deformation bands (Fig. 1A) and (2) joints, sheared joints,

and breccia (Fig. 1B). Deformation bands are tabular zones of localized deformation that are typically characterized by crushed grains, porosity loss, and shear displacement referred to as cataclasis (Fig. 1A) (Aydin and Johnson, 1978; Underhill and Woodcock, 1987). Brittle joints are planar discontinuities characterized by opening normal to the fracture plane. Joints are susceptible to reactivation in shear, which promotes the formation of new joints, called splay fractures, near the tip and oblique to the sheared joint (Cruikshank et al., 1991). Repeated formation and subsequent shearing of joints fragment the rock and lead to the formation of breccia (Flodin, 2003; Myers and Aydin, 2004). The emerging view of faults as continuously evolving zones of shear localization that form by the addition of new structures resulting from specific deformation mechanisms differs from more traditional views that considered small-scale structures as “secondary” to an established master fault or as relicts of fault nucleation (Ben-Zion and Sammis, 2003) regardless of the types of structures formed.

Davatzes et al. (2003) and Davatzes and Aydin (2003) described faults that contained both classes of structures, with joints and sheared joints consistently crosscutting—and therefore postdating—deformation bands. In addition, they showed that joints and sheared joints only occurred along some fault segments, or parts of these segments, whereas all faults described in these studies contained deformation bands.

This study was designed to determine where deformation bands and joints occur within a fault system, when they form during the fault evolution, and how they are related to fault geometry. Specifically, we attempted to resolve whether the occurrence of structures due to cataclastic deformation and brittle fracture along faults is controlled by local variations in stress conditions, e.g., as a result of fault segment interaction, or by variations in remote loading conditions. To address these problems,

[†]Present address: Earthquake Hazards Group, U.S. Geological Survey, 345 Middlefield Road, M.S. 977, Menlo Park, California 94025, USA; e-mail: ndavatzes@usgs.gov.

[‡]Present address: Texas A&M—Corpus Christi, Department of Physical and Life Sciences, 6300 Ocean Drive, Corpus Christi, Texas 78412, USA.

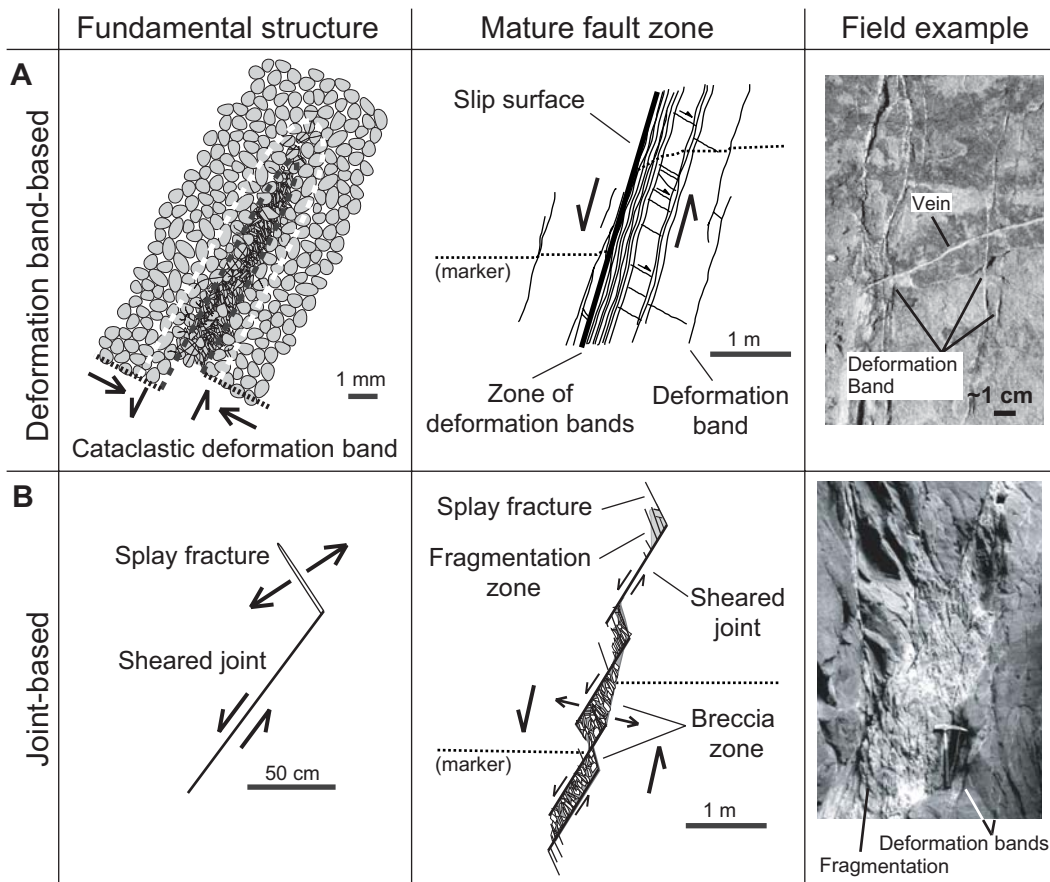


Figure 1. Two styles of faulting distinguished by the fundamental structures that compose the fault zone in sandstone: (A) Cataclastic deformation bands, a dense zone of cataclastic deformation bands, and a planar slip surface to accommodate the majority of subsequent offset. For brevity, we refer to cataclastic deformation bands simply as deformation bands in this paper. (B) Joints are discontinuities that can be easily reactivated in shear and thus promote the formation of new joints called splay fractures. Continued slip produces increasing joint density that fragments the rock and eventually produces breccia and fault rock.

we mapped the structures in sandstone along the Moab fault, southeast Utah. In addition, we conducted numerical elastic boundary element simulations to model the location and magnitude of local changes in stress state that may account for the observed temporal and spatial distribution of deformation bands and joints and sheared joints.

We demonstrate that joints are spatially associated with relays and intersections between fault segments; this fact suggests that the geometric evolution of the fault controlled where the transition from deformation band to joint formation occurred. The transition from fault growth by the formation of deformation bands to fault growth by jointing and shearing of joints, on the other hand, we attribute to the additional effects of changes in remote tectonic loading, burial depth, fluid pressure, and possibly diagenesis. Our analysis is intended to provide a physical framework of fault growth as a basis for predictive models of fault hydraulic properties and fault strength.

GEOLOGIC SETTING

The Moab fault is a 45-km-long normal fault (Fig. 2) with nearly 1 km of maximum throw

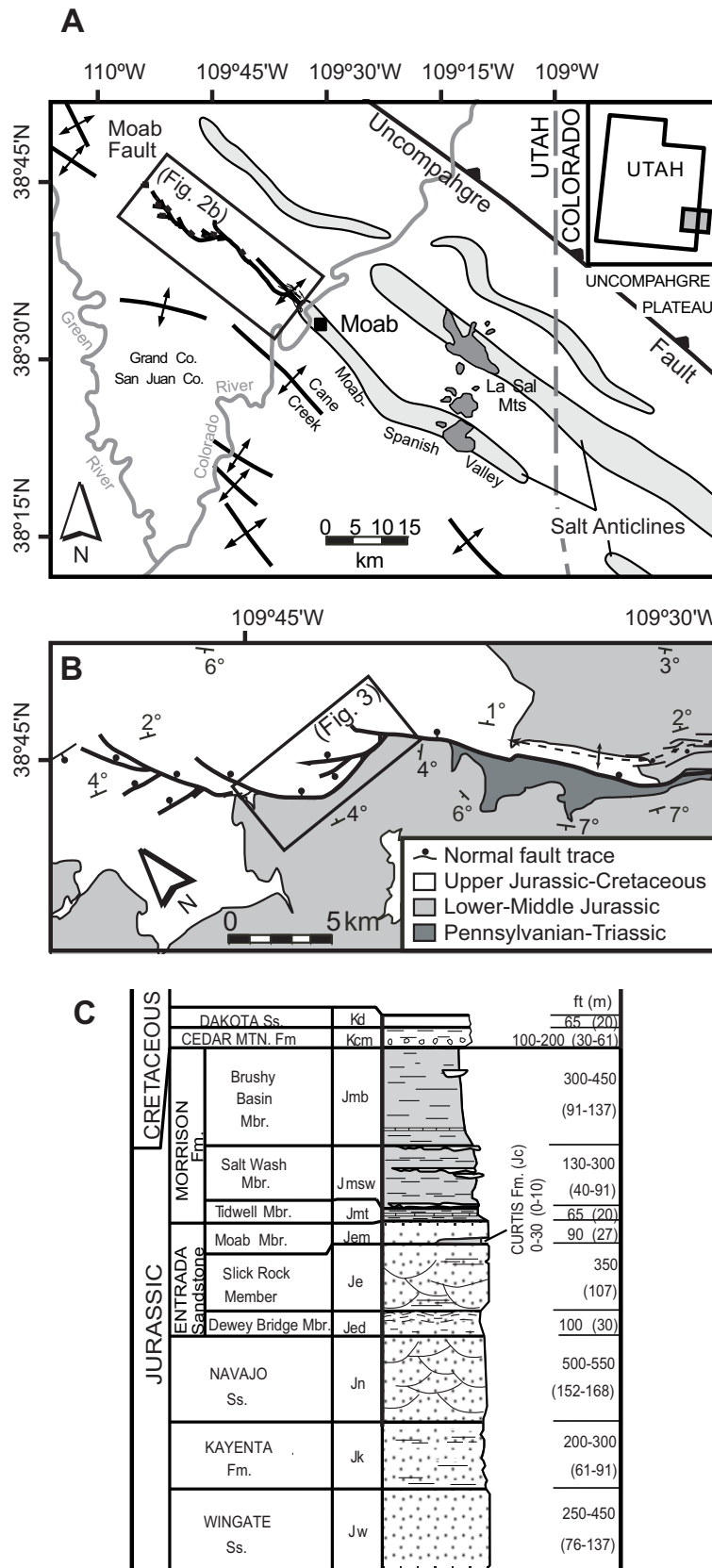
(Doelling, 1985; Foxford et al., 1996) in the Paradox Basin, southeast Utah (Fig. 2A). Pennsylvanian through Cretaceous sandstone, shale, and minor amounts of limestone are offset and exposed along the fault trace (Figs. 2B and 2C) (Doelling, 1985). Jurassic Wingate, Kayenta, Navajo, and Entrada sandstone units are exposed in the footwall along the northwest part of the fault system (Fig. 2B). The Entrada Sandstone is composed of three members: (1) the Dewey Bridge Member, (2) the Slick Rock Member, and (3) the Moab Member (Fig. 2C) (Doelling, 1988). This study focused on the deformation of high-porosity, eolian Navajo, Slick Rock, and Moab sandstone because all three units contain similar structures and are extensively exposed along the fault. Shale appears to deform by folding and pervasive shearing or smearing (Foxford et al., 1998; Davatzes and Aydin, 2004) and does not contain deformation bands or joints.

Faulting of Jurassic sandstone units in the study area probably occurred between 60 and 43 Ma on the basis of K-Ar dating of shale gouge in the Morrison Formation (Pevear and Vrolijk, 1997, and fault-related diagenesis (see Davatzes and Aydin, 2003, for a review). This faulting episode has been related to a period of

salt movement (Doelling, 1988) that occurred either during maximum burial of the Entrada Sandstone to a depth between 2000 and 2500 m (Pevear and Vrolijk, 1997; Garden et al., 2001) or during subsidence immediately preceding maximum burial (Nuccio and Condon, 1996).

In this study, we distinguish regional joint sets from joints spatially associated with the fault. These regional joint sets are characterized by consistent spacing and orientation over broad areas, which are different in each unit (Doelling, 1985, 1988). Locally, the fact that these joint sets curve in proximity to large structures such as the Salt Valley anticline and Moab fault (Dyer, 1983; Doelling, 1985; Cruikshank and Aydin, 1995; Kattenhorn et al., 2000) might indicate interaction with active faulting or the influence of the structural grain introduced by deformation bands and fault slip surfaces. Foxford et al. (1996) suggested that regional joint sets might have formed in response to regional uplift and exhumation that postdated faulting.

Joints associated with the Moab fault occur in much greater density than regional joints. The density of joints in the Navajo, Slick Rock, and Moab sandstone units away from the Moab fault is generally well below one joint every



5 m, whereas the joint density in the vicinity of the fault slip surface often exceeds 10 m in the Navajo, Slick Rock, and Moab sandstone units (Davatzes and Aydin, 2003). The strike of these joints is typically subparallel to the local strike of the Moab fault. The following description is restricted to the role of these joints in the development of the Moab fault.

FIELD METHODS

We used two techniques to quantify the distribution of deformation bands, joints, sheared joints, and breccia within sandstone units along the Moab fault. First, the frequency, orientation, and crosscutting relationships of these structures were measured along 29 scanlines normal to the fault trace. Scanlines extended from the fault trace until reaching a background structure density just outside the fault zone or until the end of outcrop exposure. We estimated a background density of less than one structure every 5 m. Second, detailed maps were made at key locations by using enlarged aerial and ground photographs on which a grid at a 1:100 scale was overlaid. Even at this scale of mapping, lines represent structure orientation and relative density rather than individual, discrete structures. We also measured the vertical offset of stratigraphic units across the fault and the rake of slickenlines on the fault slip surface to constrain the kinematic evolution of the Moab fault. These data complemented earlier offset measurements by Foxford et al. (1996).

GEOMETRY OF THE MOAB FAULT AND ALONG-STRIKE DISTRIBUTION OF STRUCTURES

The northwestern portion of the Moab fault is divided into segments along its strike by a series of relays and intersections (Fig. 3A). Three major fault segments crop out in Jurassic sandstone units. The two westernmost segments curve from a regionally dominant northwest strike (Fig. 2A) to abut against the next segment to the east. In addition, each of these segments consists of closely spaced, strike-parallel subsegments separated by relays. Subsegments consistently step to the right by 50–100 m and overlap by up to 500 m.

The relative distribution of deformation bands and joints varies along the trace of these fault segments and subsegments (Fig. 3B). Deformation bands constitute a significant proportion of the structures in the fault zone everywhere sandstone is exposed along the Moab fault. At 15 of 21 scan-line stations along fault segments with throws of >100 m, more than 90% of the structures in the fault zone are composed of

Figure 2. (A) Tectonic map of the northeast Paradox Basin (modified from Doelling, 1985). (B) Map of the Moab normal fault system (modified from Foxford et al., 1996). (C) Stratigraphic column of the Jurassic section including units mapped in subsequent figures.

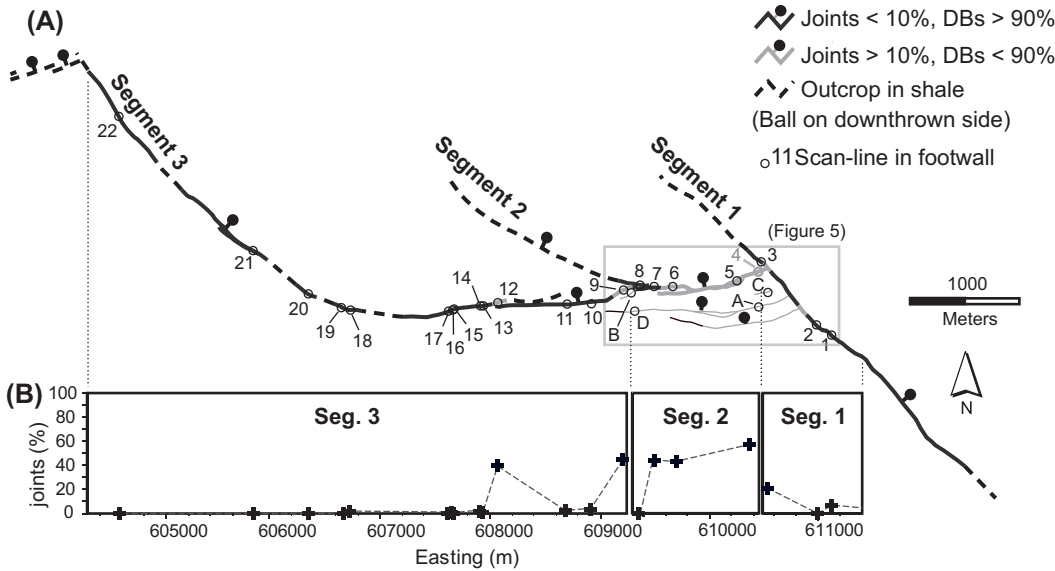


Figure 3. (A) Index map of fault segments composing the north-west extension of the Moab fault system with locations where data were collected along scanlines. (B) Plots depict the percentage of structures that formed as joints, as opposed to deformation bands (DBs), in the fault zone of normal fault segments 1, 2, and 3, which have throws of >100 m. The position of each station is indicated in UTM coordinates, zone 12 N, NAD83. Detailed data from stations 5 and C are presented in Davatzes and Aydin (2003); data for stations 3, 4, 6, 8, and 9 are available from an online data repository as Figures DR1–DR4.

deformation bands. At the remaining six stations, joint-related structures constitute a large percentage of the structures. These stations are distinguished from deformation band-dominated stations by the proximity of relays and intersections between fault segments. The association of fault geometry and fault zone structures also remains consistent in all sandstone units exposed in the region (e.g., Figs. 4 and 5). Overall, the density of both deformation bands and joints is highest adjacent to intersections and in relays between fault segments, especially within 10 m of the fault slip surfaces (Figs. 4 and 5). Several subsidiary faults with <25 m of throw (mapped as thin lines in Fig. 3A) demonstrate the same relationship between fault segmentation and the occurrence of joint-based structures (Fig. 4). However in these examples, segmentation occurs at a much finer length scale, ~5–10 m, than is apparent along the main fault segments. Furthermore, the vertical exposure provided by canyon walls >50 m high in the Entrada Sandstone also illustrate the importance of segmentation along dip as well as strike (see Fig. 11 in Davatzes and Aydin, 2003).

THE RELATIONSHIP OF FAULT GEOMETRY AND KINEMATICS TO STRUCTURES

For a quantitative comparison of the fault geometry and kinematics with the distribution and orientation of deformation bands and joints, we mapped these structures in the fault zone at two intersections and two relays (Fig. 5). Later in this paper we use these kine-

matic and geometric constraints to simulate the local state of stress around the fault for comparison to the relative distribution of deformation bands vs. joints.

Relays

Relays between normal fault subsegments along the Moab fault locally demonstrate significant strike-slip components that may reach 15%–25% of the throw, equivalent to a rake that diverges by ~10°–15° from pure dip slip. At the relay east of Mill Canyon (Figs. 5 and 6A), slickenlines on the fault segments that define the relay have an average rake of ~80° from the east (Fig. 7B). These rakes correspond to a left-lateral strike-slip component, which, in a right-stepping relay, produces extension parallel to fault strike. Deformation bands, joints, and sheared joints are distributed across the entire relay. The highest density of deformation bands occurs within the relay adjacent and parallel to the bounding fault segments (Figs. 6A and quantified in a frequency plot in Fig. DR1)¹ and comprise the core of these faults. Joints consistently overprint deformation bands and primarily occur within, and not outside, the relay. The joints are most densely developed immediately adjacent to subsegment 2b (Fig. 6A) where they fragment

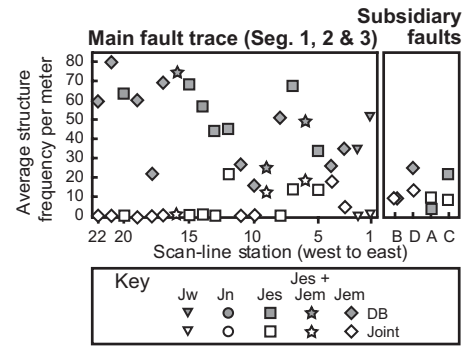


Figure 4. The average density of deformation bands and joints within 10 m of the fault surface at each station.

the rock and strike parallel to the bounding fault segments. The joints in the interior of the relay, and away from the bounding faults, are consistently oblique to the strike of the bounding faults.

In contrast to the extensional relay east of Mill Canyon, the relay west of Mill Canyon (Figs. 5 and 6B) is contractional parallel to fault strike. Although also right-stepping, slickenlines on the bounding fault segments have an average rake of ~80° from the west (Fig. 7B), which corresponds to a right-lateral strike-slip component and which produces the strike-parallel contraction. Unlike the extensional relay, joints are absent within the contractional relay. Instead, the core of each bounding fault segment is solely composed

¹GSA Data Repository item 2005025, Figures DR1–DR4, is available on the Web at <http://www.geosociety.org/pubs/ft2005.htm>. Requests may also be sent to editing@geosociety.org.

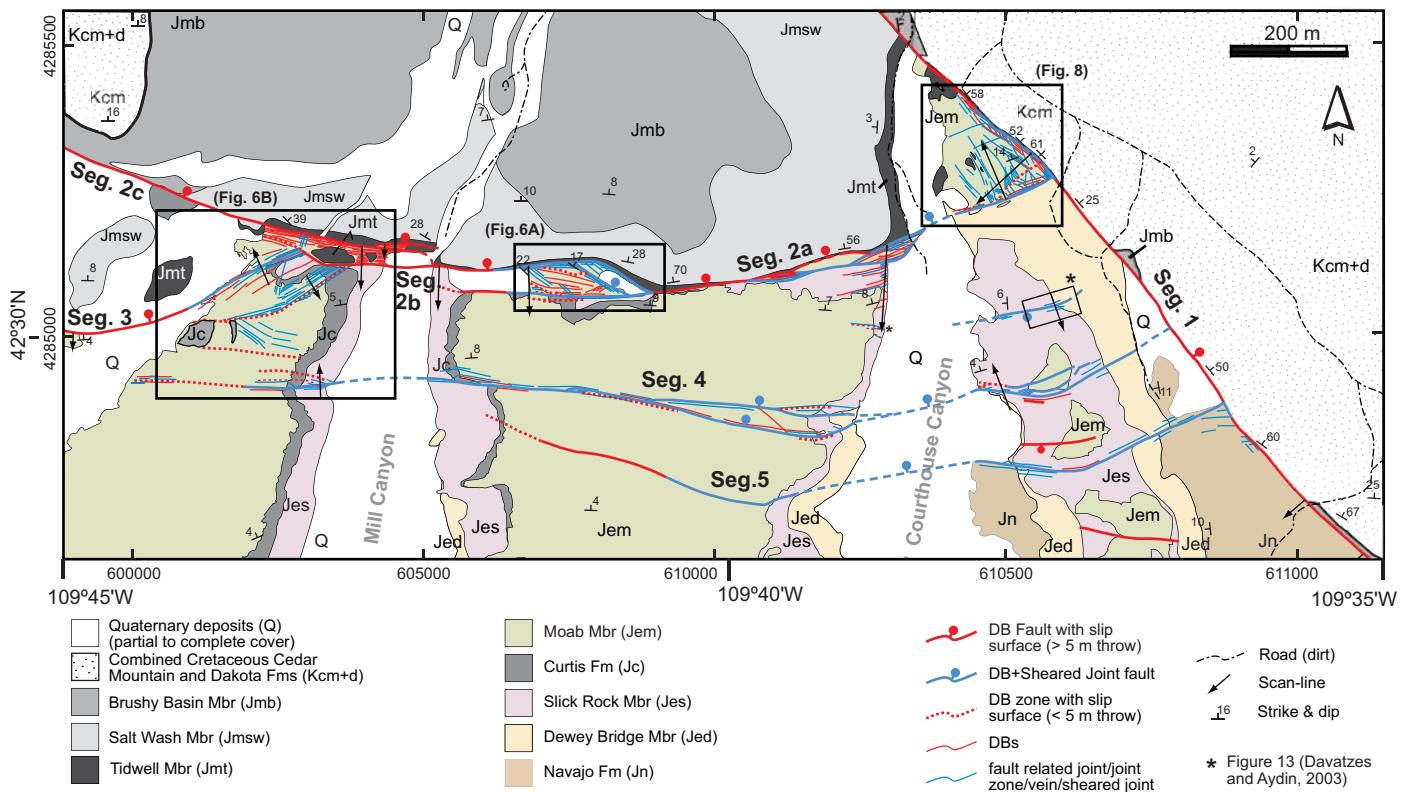


Figure 5. Geologic map showing the distribution of structures in the fault zone. Locations of Figures 6 and 8 are indicated. Distinct segments separated by intersections are numbered for reference in the text. Note that segment 2 is broken into multiple subsegments by relays that are referred to as segment 2a, 2b, or 2c.

of a dense zone of deformation bands with an adjacent slip surface. More deformation bands parallel to the bounding faults are distributed across the entire relay (Fig. 6B; frequency plot in Fig. DR2 [see footnote 1]).

Intersections

The structural and kinematic features of intersections are most prominently displayed in Courthouse Canyon along the intersection of segment 2 with segment 1 (Figs. 5 and 8) and near Mill Canyon at two intersections including segment 3 with segment 2 and a small fault with 7 m of throw that also abuts segment 2 (Figs. 5 and 6B). Each of these intersections is associated with large densities of deformation bands overprinted by joints, sheared joints, and splay fractures in all of the exposed sandstone units (Figs. 6B and 8, frequency plots in Figs. DR3 and DR4 [see footnote 1]). Breccia and the largest joint densities occur along the abutting faults. In addition, joints occur primarily in the hanging wall of the abutting segment at all three intersections. Joints are dominantly oriented parallel to the fault segments at each

intersection (stereograms in Figs. DR3 and DR4). At Mill Canyon (Fig. 6B), many joints project beyond the intersection into the hanging wall of subsegment 2b, where joint strike ranges within $\pm 30^\circ$ of the strike of segment 3. In addition to the localized joint occurrence, intersections are spatially associated with large gradients in the rake of slickenlines and fault throw over short distances along fault strike (Fig. 7, intersections indicated by vertical dashed lines).

Lateral Fault Tips

Just west of Mill Canyon (in the southwestern part of Fig. 6B), joints are spatially associated with the lateral tip of a small fault (segment 4). The joints are confined to the region in the footwall just south of the fault tip. At this location, segment 4 is predominantly dip slip with a component of left-lateral strike slip indicated by a rake of 80° from the west. The strike-parallel component of slip indicates a component of extension in the footwall area near the fault tip, which is consistent with the distribution of joints.

MECHANICAL ANALYSIS OF THE DISTRIBUTION OF STRUCTURES

The field observations indicate that joints and sheared joints are restricted to locations of complex fault geometry, such as relays, intersections, and fault tips, where they consistently overprint deformation bands. The fact that each of these locations is associated with gradients in the rake of slickenlines and throw along fault strike suggests that the distribution of joints and sheared joints in the fault zone is controlled by fault kinematics. This kinematic control is most clearly demonstrated by the occurrence of joints in relays of strike-parallel extension and their absence in relays of strike-parallel contraction. Their occurrence in extensional, rather than contractional, relays is consistent with the formation of joints as a result of an effectively tensile local least compressive principal stress (Pollard and Aydin, 1988). In contrast to the joints, the deformation bands along the Moab fault exhibit porosity reduction, which suggests volume loss and contraction, and thus are not favored under conditions of effective tension. Although, the formation of deformation bands is not easily

related to a single stress parameter (Issen and Rudnicki, 2000), mean stress (σ_m) can be used to distinguish areas that favor dilation from areas that favor contraction (Pollard and Segall, 1987). Thus, increases in mean stress provide a proxy for conditions that favor deformation band formation as opposed to joints.

We postulate that fault tips, relays, and intersections perturbed the local state of stress and thus controlled the distribution of joints and sheared joints during development of the Moab fault zone. As a test, we performed mechanical simulations that predict the local state of stress and compared results from these simulations to the mapped distribution of joints and sheared joints. These simulations are based on the premise that changes in the local state of stress along the fault are a function of the kinematics of slip, which is controlled by the geometry of a fault system and the remote state of stress.

We developed two sets of mechanical models. First, we modeled the entire Moab fault system to find a remote stress state that is consistent with the geometry and the measured distribution of throw and the rake of slickenlines. Second, we examined simplified models of relays and intersections between fault segments subjected to the remote stress boundary conditions derived from the previous analysis.

Numerical solutions were obtained by using Poly3D (Thomas, 1993), a three-dimensional boundary element code based on the displacement-discontinuity method. In this program, a fault is defined by boundary surfaces discretized into triangular dislocations within a linear elastic, homogeneous, and isotropic continuum. Solutions using this program are quasi-static.

Constraints on the Remote State of Stress

The boundary conditions for the numerical simulations include (1) the geometry of the fault, (2) traction and displacement on the simulated fault surfaces, (3) the elastic properties of the rock, and (4) the remote stress state. We constrained the fault geometry with our field maps in combination with published geologic maps and measured sections (Doelling, 1982, 1988) and publicly available well data. The lower fault tip was generally chosen to intersect the top of the Paradox salt, consistent with the well data, inferred slip distribution at depth, and published cross sections (Doelling, 1988). The partially eroded upper tip was assumed to occur in overlying shale of the Morrison Formation and Mancos Shale, consistent with mapped examples along the northwest parts of the fault system. In addition, the height of the Moab fault is greater than its depth of burial; thus we include the effect of the Earth's surface in our model.

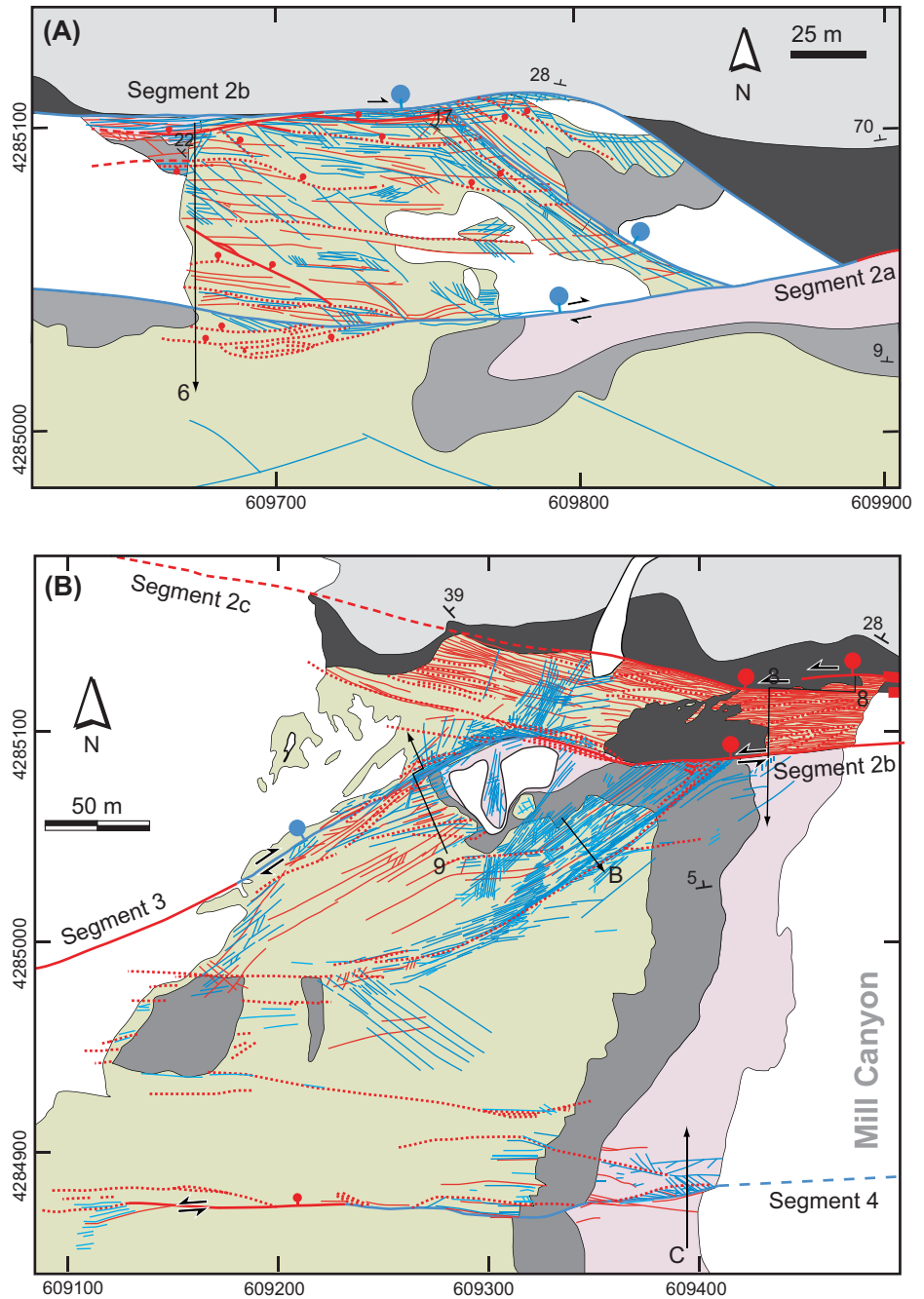


Figure 6. (A) Map of the structures at the relay between normal fault segments 2a and 2b. (B) Map of structures at the relay between (upper right) segments 2b and 2c and (center) an intersection between segments 2 and 3. Legend as in Figure 5.

Traction and displacement boundary conditions include the simplifying assumptions of a complete shear stress drop across fault surfaces without opening or interpenetration. We selected elastic rock properties consistent with the range of sedimentary rocks (Jaeger and Cook, 1979; Bieniawski, 1984): we used

20 GPa for Young's modulus and 0.25 for Poisson's ratio. The impact of variation in these parameters is discussed by Bürgman et al. (1994) and Bourne and Willemse (2001).

Remote stress boundary conditions were chosen consistent with the ~2 km depth during fault activity of the now-exhumed Entrada

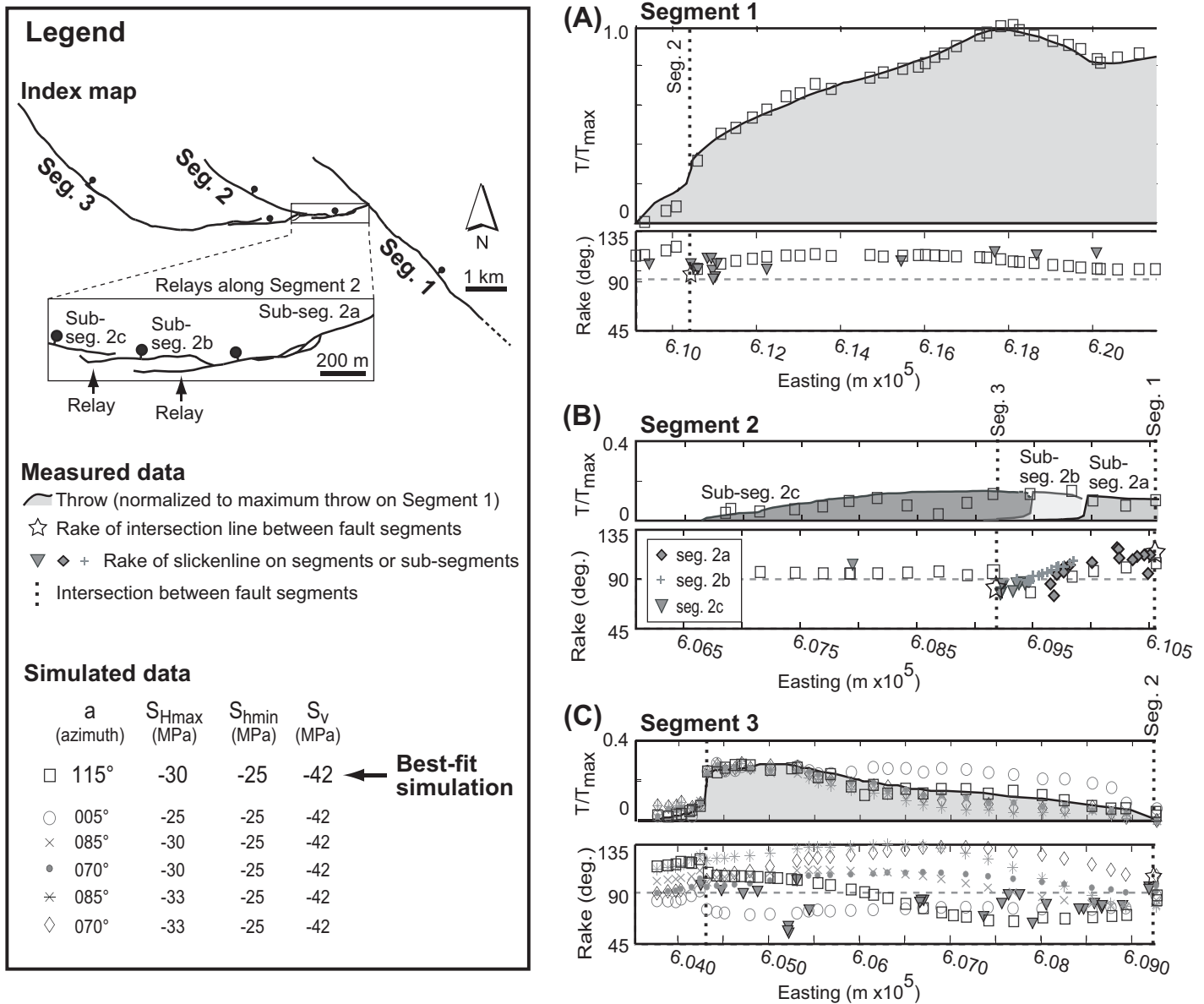


Figure 7. Plots of the measured throw (T , normalized to maximum throw, T_{max} , on segment 1) and rake of slickenlines along (A) segment 1, (B) segment 2, and (C) segment 3. Estimates of fault throw are modified from Foxford et al. (1996). Results from mechanical simulations are superimposed on the field data for comparison. The parameter a refers to the azimuth of S_{hmin} .

Sandstone. Because normal faulting is dominant, we assumed that the vertical stress represents the remote maximum compressive stress (Anderson, 1951) and is equal to the weight of the overburden. Assuming a uniform overburden density of 2.1 g/cm^3 , representative of sedimentary rocks (Mavko et al., 1998), yielded a vertical stress of 42 MPa (compression positive). We neglect variations of stress with depth because our field analysis is limited to a single depth within the fault system. The minimum horizontal compressive stress, S_{hmin} , is assumed

to be proportional to the vertical stress magnitude, S_v , so that $S_{hmin} = 0.6S_v$.

Because the azimuth and magnitude of S_{hmax} are not known a priori, we systematically varied the azimuth between 365° and 175° and the magnitude between the magnitudes of S_{hmin} and S_v , and we calculated the resulting distribution of throw and rake of slip along the fault. The results were then compared to the measured distribution of throw and the rake of slickenlines (Fig. 7). This analysis is based on the assumption that the rake of slickenlines

corresponds to the direction of maximum shear traction resolved on the fault plane (Bott, 1959; Angelier, 1994). We also required a single stress state that produces the best fit to the throw distribution and rake of slickenlines along all fault segments, which assumes that all faults slipped in a uniform remote stress state.

We found that the best fit to kinematic data from fault segments 1, 2, and 3 was produced with an S_{hmin} orientation of 115° and an S_{hmax} magnitude of 30 MPa (Fig. 7). Figure 7C depicts results from several realizations of slip

along segment 3. This segment is particularly sensitive to the remote stress state because it changes strike by over 60°, and portions of the faults are isolated from other segments, which minimizes mechanical interaction. These results in Figure 7C indicate that only a narrow range of principal stress ratios and orientations produce reasonable fits with the available throw distribution, rake, and fault geometry data sets.

Unlike previous techniques that use kinematic data to infer the stress state during the evolution of ancient faults (e.g., Angelier, 1994), the approach used in this study accounts for the elastic interaction of slipping fault segments. In addition, the elastic interaction is sensitive to the ratio of remote principal stresses and thus provides additional information to constrain estimates of the remote stress state, thereby allowing a robust estimate from limited data sets.

Results from Simplified Fault Models

To evaluate the occurrence and distribution of effective tensile stress, necessary for joint formation, we simulated the local state of stress associated with geometrically simplified relays and intersections by using the remote stress state derived above. Specifically, downdip constraints on fault geometry are limited, so we have simplified the models presented here to have uniform geometry along dip. Furthermore, they allow greater mesh density, which is necessary to examine the stress state close to fault segments separated by intersections and narrow relays.

Simulations of Relays

Models of relays are composed of two en echelon, right-stepping, rectangular normal faults dipping 70° to the north and striking 270°. Each fault is 1000 m long and 2000 m tall, which isolates the observation level from outertip effects. We tested cases with distinct fault segments as well as cases in which the relay has been breached, because we postulate that relays that are now breached were presumably unbreached at an earlier stage. The remote stress state applied in the simulations of the extensional and the contractional relays were based on the simulation of the entire fault system. This approach accounts for the elastic interactions of segments 1 and 2. For the extensional relay, the remote stress state corresponds to an azimuth of $S_{H_{max}}$ of 105°, whereas for the contractional relay, $S_{H_{max}}$ is oriented at an azimuth of 075°, with a magnitude of 30 MPa in both cases.

In the extensional relay, the right-lateral component of strike slip, in combination with the normal slip, produces a less compressive mean stress, σ_m (Figs. 9A and 9B), and a

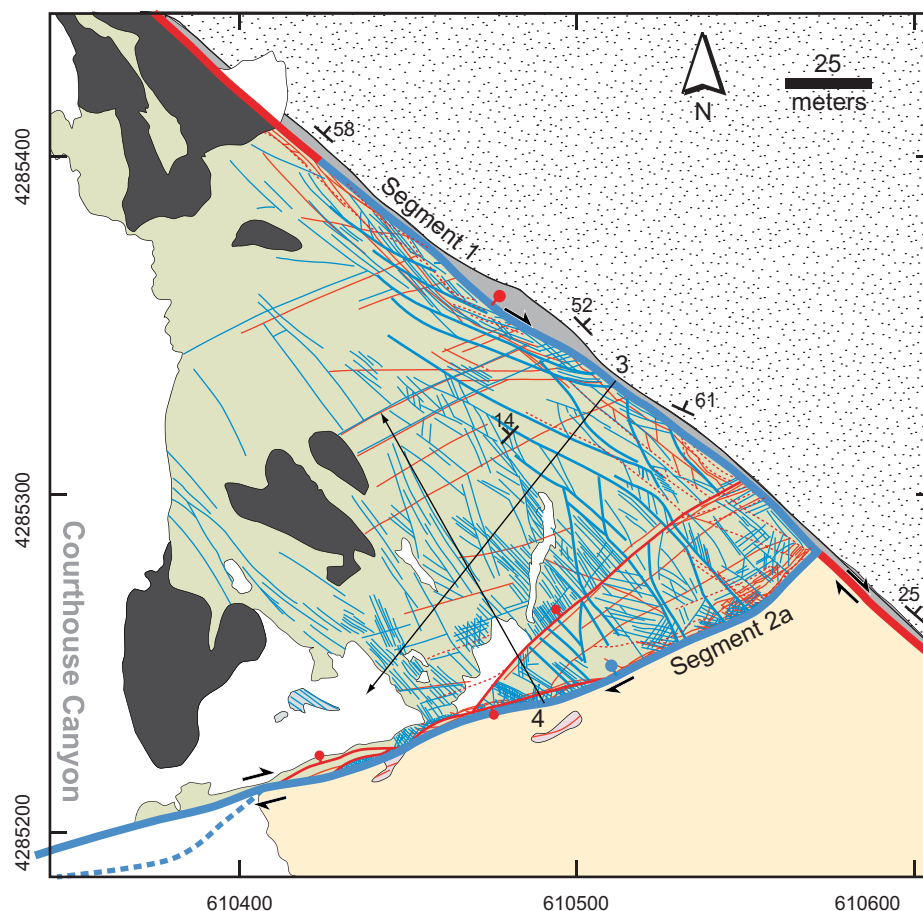


Figure 8. Structures at the intersection of segment 2 with segment 1. See locations in Figure 4. Legend as in Figure 5.

less compressive, and thus more tensile, least compressive principal stress, σ_3 (Figs. 9C and 9D), within the relay. Both effects are more pronounced in the unbreached case than in the breached case (e.g., Figs. 9C and 9D). Overall, the more tensile σ_3 and σ_m within the relay would favor joint formation and tend to suppress the formation of deformation bands that accommodate compaction. In both the unbreached and breached realizations, the orientation of σ_3 predicts that joints would dip steeply and strike northwest, consistent with the joint orientation observed in the field in the interior of the relay (Figs. 6A and Fig. DR1).

In contrast, in the contractional relay, the component of left-lateral strike slip produces more compressive σ_m (Figs. 9E and 9F) and σ_3 for both unbreached and breached geometries, which would favor deformation band formation and inhibit joint formation. This situation is consistent with the high density of deformation bands localized within the contractional relay in Figure 6B.

Simulations of Intersections

Our model intersection is composed of two fault segments, a throughgoing and an abutting segment (Fig. 10A), with rectangular tip lines (except along the intersection) and equal height, which dip 70° and intersect at a 60° angle—similar to the intersection of segment 2 with segment 1 (Fig. 8). Each fault segment is 3000 m tall consistent with published cross sections (Doelling, 1988). The trace length of the throughgoing segment is 15,000 m, similar to the mapped fault trace. The upper tip of each fault is ~2 km below the Earth's surface. The throughgoing fault segment strikes 320°, the abutting segment strikes 260°, and the remote stress state is as derived in Figure 7, and $S_{H_{max}}$ are oriented at an azimuth of 025° with a magnitude of 30 MPa.

In this simulation, both σ_m and σ_3 become more tensile over a limited region in the hanging wall of the abutting segment west of the intersection (Figs. 10B and 10C), which favors joint formation consistent with the occurrence

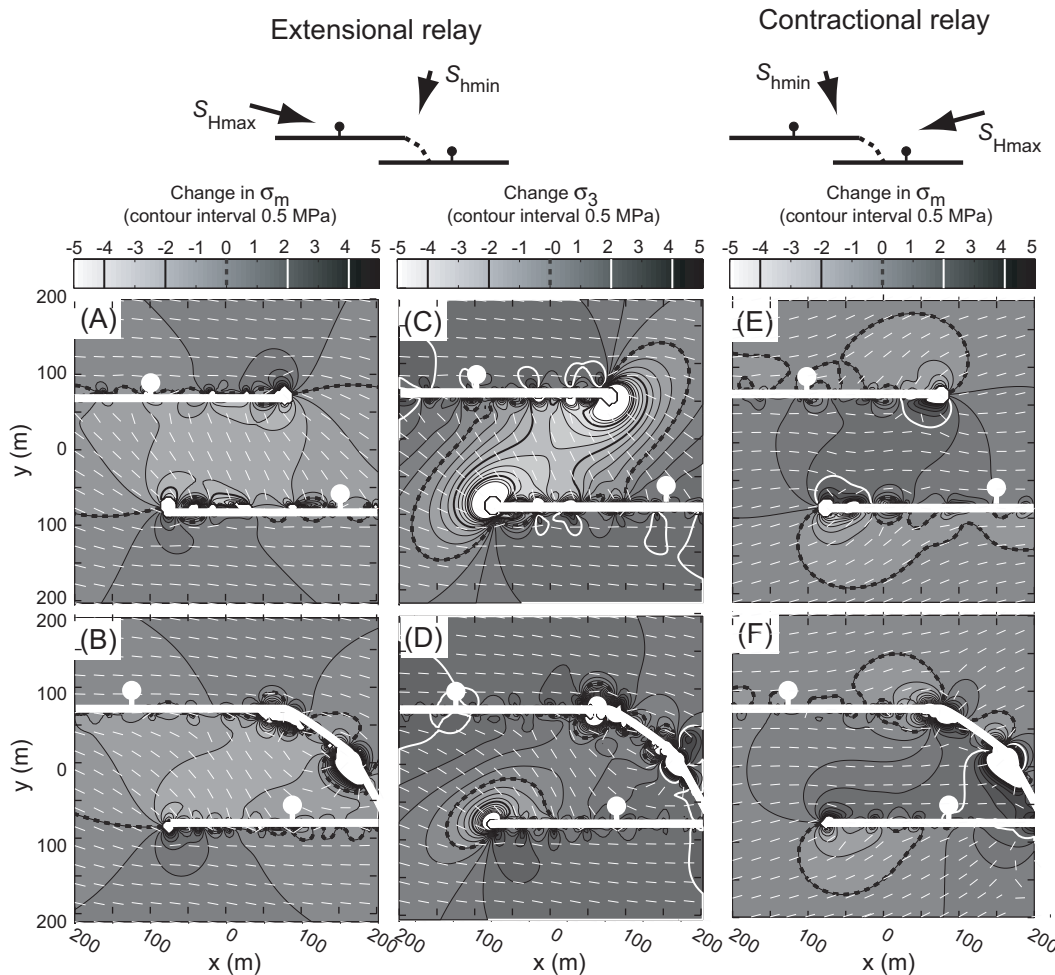


Figure 9. Contour plots corresponding to the two stress states: S_{hmin} oriented 015° and 345° . Immediately adjacent to modeled faults, numerical artifacts result from the singularity at the edge of elements defining the faults. (A–D) S_{hmin} oriented 015° . Contours of change in σ_m for (A) an unbreached and (B) a breached relay, and contours of the change in least compressive principal stress, σ_3 for (C) the unbreached and (D) breached relays. (E–F) S_{hmin} oriented 345° . Contours of the change in mean stress for (E) an unbreached and (F) a breached relay fault geometry. Tick marks are normal to σ_3 and thus parallel the predicted orientations of joints in the total stress state.

of joints in this location (Figs. 6B and 8). These joints are predicted to dip steeply and strike at an azimuth of 340° consistent with the observed orientation (Fig. 8, Fig. DR3 and DR4). Another region of more tensile σ_m and σ_3 occurs in the hanging wall of the throughgoing fault segment opposite the intersection with the abutting fault segment. This location corresponds to an intensely jointed region at the intersection of segment 3 with segment 2 (Fig. 6B). The predicted orientation of these joints is consistent with the observed joint orientation relative to the strike of the fault segments (Fig. 6B). The corresponding location at the intersection of segment 2 with segment 1 (Fig. 8) is exposed in shale where joints are not observed.

The occurrence of joints in the hanging wall of the abutting segment depends on the orientation of the remote stresses, such that σ_3 becomes more tensile over an S_{Hmax} azimuth range from 350° to 050° (Fig. 10D, region 1). A more tensile σ_3 in the hanging wall of the throughgoing

fault segment is essentially independent of the S_{Hmax} orientation (Fig. 10D, region 3). In the footwall of the abutting fault segment, σ_3 is always more compressive (Fig. 10C, region 2) irrespective of S_{Hmax} orientation.

Sensitivity of σ_3 to Fault Height and Burial Depth

The qualitative trends in the stress perturbation described above are independent of scale. However, the physical extent of the perturbation depends on the fault dimensions and primarily on the shortest dimension, which is the height. In addition, depth of burial is another important scaling property because the Earth's surface is traction free and because S_v scales with depth. We tested the sensitivity of σ_3 to fault height and burial depth because these parameters are two of the least constrained parameters in our simulations. In addition, these are parameters that have likely changed during fault evolution and thus might be of interest for explaining the relative ages of deformation bands and joints

in the fault zone. Because the results apply to both relays and intersections equally, we only show the results from simulations of intersections for brevity.

In the trivial case where the height of all fault segments increases proportionally, the extent of the stress perturbation increases linearly with fault height. More interesting is the case where fault segments grow at different rates, which is also probable for natural faults. To examine this effect on a simple intersection, we varied the ratio of the height of the abutting segment relative to the fixed height of the throughgoing segment. As the height of the abutting segment increases and approaches the height of the throughgoing segment, the magnitude of σ_3 becomes increasingly tensile in regions 1 and 3 of Figure 11A, which correspond to jointed regions in the field. This scenario predicts that region 1 would initially favor deformation band formation. However, as the height of the abutting fault segment increases, joint formation becomes more favored in region 1.

The effect of the depth of burial on the stress perturbation was modeled for constant fault geometry by assuming that the horizontal stresses remain linearly proportional to S_v , which is a function of depth. In regions 1 and 3, the magnitude of σ_3 is most tensile at shallow depths and becomes less tensile at a rate that decreases with depth (Fig. 11B). If we assume a hydrostatic-pore-fluid pressure gradient, σ_3 becomes effectively tensile in region 3 and in part of region 1.

DISCUSSION

Development of the Moab Fault Zone in Sandstone

Cataclastic deformation bands are the primary structure everywhere the Moab fault zone is exposed in sandstone. Even in locations where brittle joints and sheared joints occur, they overprint deformation bands, indicating that the overall geometry of the fault system was established by the deformation bands (Fig. 12A). Consequently, joints must have formed at a late stage in the development of the fault system. The geometry established by deformation bands, in combination with the remote stress state derived from the rake and throw distributions (Fig. 7), produced more tensile σ_3 and σ_m (Figs. 9 and 10) in extensional fault relays, intersections, and tips where the highest joint density is observed (Fig. 3). Whereas continued fault slip at these locations was accommodated by joints and their subsequent shearing, slip along the remainder of the fault was associated with more compressive σ_m , resulting in the continued formation of deformation bands (Figs. 12B and 12C).

The final distribution of joints and their orientation are consistent with the perturbed stress state associated with the local mechanical interaction of fault segments. Although we cannot establish whether the transition from deformation band to joint formation occurred concurrently at each of these locations (Fig. 5), the consistent overprinting relationship indicates a change in the boundary conditions affecting the fault system. Changes in boundary conditions important to this transition include changes to (1) the remote stress state, (2) the material properties, and (3) the fault dimensions. Changes in remote stress may result from changes in burial depth, fluid pressure, and regional tectonics. Uplift and exhumation would reduce the remote mean stress proportional to the change in depth and move the fault closer to the traction-free surface of the Earth. It is possible that Moab fault activity extended into the period of uplift and erosion that began at ca. 40 Ma (Nuccio and Condon, 1996; Garden

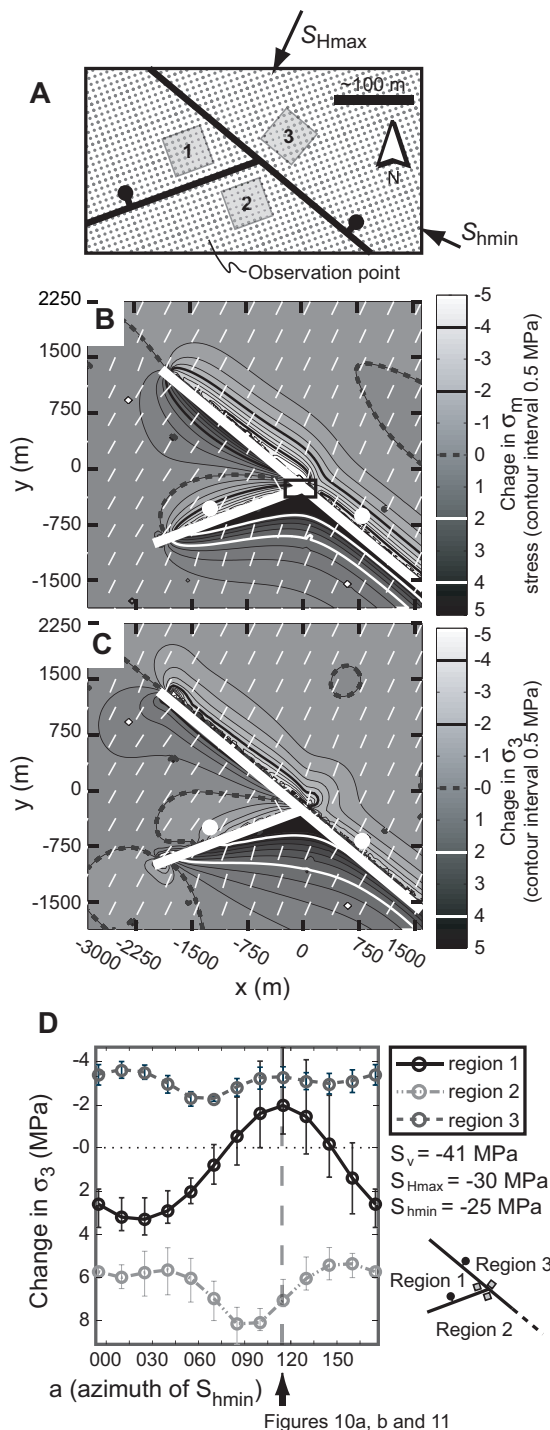


Figure 10. (A) Map-view illustration of model geometry including dots that represent observations points used to contour the local state of stress. Boxed regions: region 1 corresponds to the discrete jointed area in Figure 8, region 2 to the jointed area in Figure 6B, and region 3 to an unjointed area in Figure 8 for comparison with the other two regions. The distance of each region from the fault is the distance over which the elastic solution is nonphysical owing to the stress singularity associated with element edges in the model. (B) Contour plot of the change in σ_m and (C) contour plot of the change in σ_3 . Tick marks are normal to the least compressive principal stress and thus parallel the predicted orientations of joints from the total stress state. (D) The impact of stress rotation on the magnitude of the stress perturbation in three key regions around the simulated fault intersections. The data plotted are the average for each region, whereas the error bars indicate the range of values in these regions.

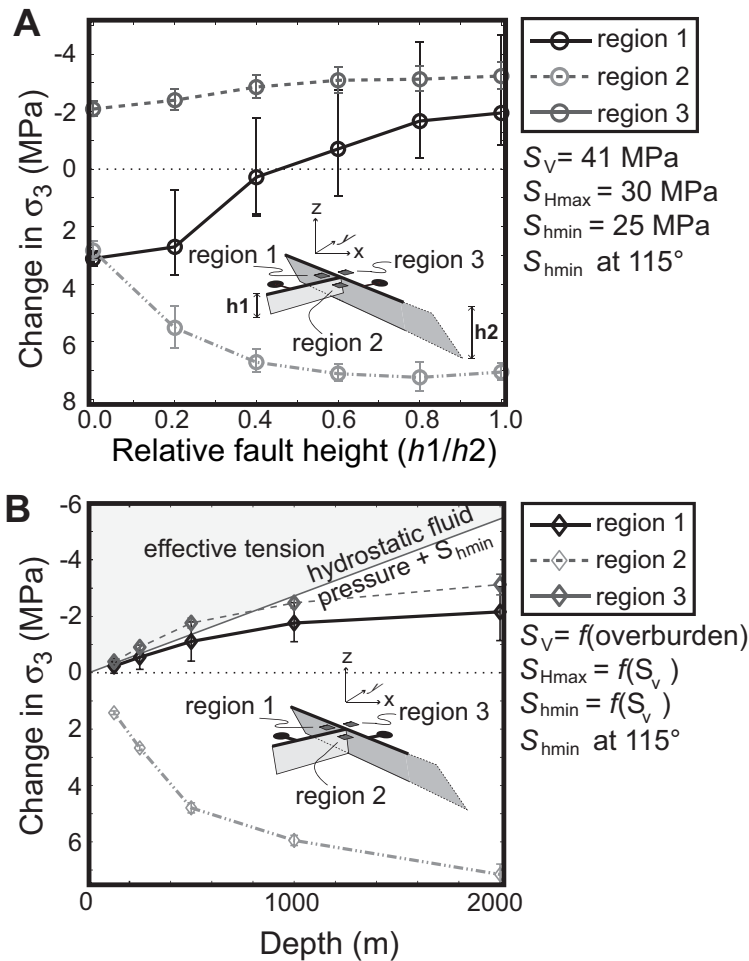


Figure 11. (A) Plot of the relative height of fault segments vs. the change in least compressive principal stress, σ_3 , at three key locations around a fault intersection. (B) Plot of depth vs. the change in the σ_3 magnitude at three key locations around a fault intersection. The faults at each depth are loaded by using the same ratio of S_{Hmin} and S_{Hmax} to S_v as described in the text and used for Figure 10. S_v is calculated from the overburden thickness.

et al., 2001). As shown in Figure 11B, regions where joints are observed approach effective tension because of exhumation, and regions 1 and 3 reach effective tension even under a hydrostatic-pore-fluid pressure gradient. As the remote mean stress becomes less compressive, the perturbation associated with the fault geometry becomes more dominant in controlling the local stress state. Alternatively, just an increase in fluid pressure gradient could cause the transition to joint formation, which would first occur in regions already favored by the perturbed stress state owing to mechanical interaction. Regional tectonic processes (Davatzes and Aydin, 2003) including the transition from the Sevier- to the Laramide-style faulting (Hintze, 1993), as well as salt movement in the underlying Paradox Formation (Doelling, 1988), could have changed the stress state during faulting.

Although the rake of slickenlines possibly only represents the most recent stages of faulting, the throw represents the cumulative history of slip. Our fit to these kinematic data suggests that the Moab fault underwent a reasonably simple loading history, characterized by small changes in the remote stress state. This interpretation is also consistent with the lack of evidence that the sense of slip on the fault significantly changed over time.

Rock properties such as porosity have been identified as a control on the occurrence of deformation bands (Antonellini et al., 1994). Thus loss of porosity due to compaction with increasing burial depth and diagenesis could be related to a transition from deformation band to joint formation. However, the occurrence of joints does not appear to correlate with porosity, or other characteristics such as grain size,

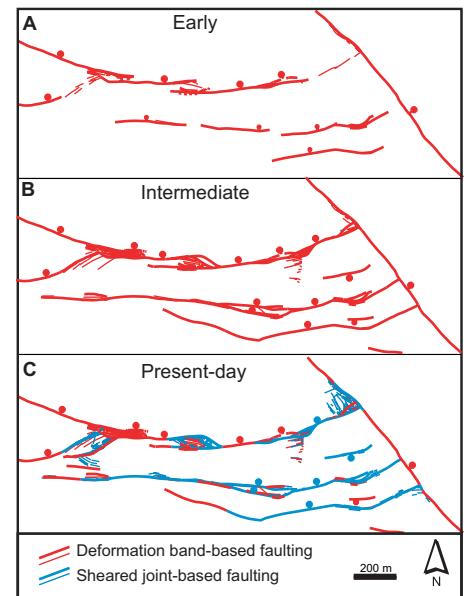


Figure 12. Interpreted development of the Moab fault system distinguishing three stages: (A) development of fault geometry by the formation of deformation bands; (B) continued geometric development leading to locally high deformation band density and a well-developed fault geometry; (C) formation of joints at relays, intersections, and fault tips, although joints need not form in all areas concurrently, and the formation of deformation bands along the remainder of the fault.

within a single sandstone unit, or among the three sandstone units exposed along the Moab fault and mapped in this study. Furthermore, the fact that deformation bands cross changes in porosity and grain size associated with small-scale sedimentary structures suggests that these properties do not vary sufficiently to inhibit the occurrence of deformation bands along the Moab fault. Changes in rock properties could also result from the cementation of sandstone as observed along portions of the fault (Foxford et al., 1996, 1998). However, joint occurrence does not appear to uniquely correlate with cement occurrence: joints also occur where cement is absent, where cement seals joints, or where veins are undeformed and thus postdate their formation.

In addition, the introduction of new structures could also cause changes to the mechanical properties of rock in the fault zone. Joints are discontinuities lacking cohesion that can slide or open. The occurrence of joints can thus reduce the effective, or bulk, stiffness of rock (e.g., Mavko et al., 1998) as well as reduce the rock

strength. This situation amounts to a “softening” of the rock that might localize strain in jointed regions, which provides a positive feedback promoting the formation of new joints as fault slip continues. In contrast, deformation bands preserve the cohesion of the rock mass and might increase the rock stiffness by strain hardening due to the increased number of grain contacts accompanying grain crushing and porosity loss in the bands (e.g., Aydin and Johnson, 1978; Menendez et al., 1996). This possibility suggests that the strength of the Moab fault zone might have varied because of the types and densities of structures in the fault zone.

Changes in fault dimensions affect the transition from deformation band to joint formation by controlling the area over which stresses are dominated by mechanical interaction between fault segments. The jointed region at the intersection of segments 1 and 2 (region 1 in Fig. 11A) becomes more tensile than the remote stress only when the abutting fault, segment 2, is greater than about one-half the height of the throughgoing fault, segment 1. Thus, the areas prone to joint formation are expected to change as the fault grows, suggesting that the transition from deformation band to joint formation may not have occurred at the same time at different locations along the fault. The stress perturbation at relays is similarly affected by the overlap distance, spacing, and relative strike and dip dimensions of fault segments (e.g., Willemsse et al., 1996; Crider and Pollard, 1998; Kattenhorn and Pollard, 1999). In general, greater overlap and closer spacing between fault segments relative to their dimensions accompanying fault growth increases fault interaction and the accompanying stress perturbation. These processes also provide a means for local rotations of the stress field that are necessary to reactivate joints in shear.

Implications for the Evolution of Faults in Sandstone

The evolution of structures in a fault zone during the nucleation of faults and their continued growth has been the subject of considerable research summarized in papers by Crider and Peacock (2004) and Kim et al. (2004). These reviews primarily focused on describing the geometry and sequence of structures that develop during fault nucleation or develop at different locations on a fault as slip accumulates. The process of forming faults in the upper crust appears to be dominated either by semibrittle shear zones, such as deformation bands, or by pre-existing or early-formed brittle structures that locally perturb the stress state and link to localize subsequent shear

and allow fault growth (Davatzes et al., 2003; Davatzes and Aydin, 2003; Myers and Aydin, 2004; Crider and Peacock, 2004). At the Moab fault, established structures, such as deformation bands or joints, are continually involved in fault development, and their presence has influenced the type, geometry, and occurrence of younger structures formed in the fault zone. Thus, fault development by (1) the formation of deformation bands or (2) the formation and shearing of joints defines two basic mechanisms of faulting in sandstone that produce faults with distinct assemblages of structures (Davatzes and Aydin, 2003) as outlined for simple faults in Figure 1. In this study we demonstrated that the basic structures formed by these two mechanisms—one defined by the formation of cataclastic deformation bands (Aydin and Johnson, 1978) and the other defined by the formation of brittle joints and shearing of these joints (Segall and Pollard, 1983; Martel et al., 1988; Myers and Aydin, 2004; Flodin and Aydin, 2004)—are related to the stress state that locally varies along a fault. By extension, changes to the local stress state determine how much slip each mechanism accommodates and thus the relative abundance of deformation bands or joints in the fault zone (Davatzes et al., 2003; Davatzes and Aydin, 2003).

Our results provide evidence that the structural patterns in Figures 5, 6, and 8 systematically evolved because of changes in fault geometry—including the development of fault segments, relays, and intersections—and changes in remote boundary conditions resulting from burial and exhumation, tectonic processes, and fluid pressure. In general, these results suggest that changes in the type and geometry of fault zone structures will most likely be initiated and will be most pronounced at fault relays, intersections, and tips where they will be associated with distinct slip kinematics. This explanation is consistent with field examples summarized by Kim et al. (2004), who related the distribution and geometry of structures around a fault to the position relative to the fault tip and to the sense of slip relative to the orientation of the fault tip-line. However, our results on joint formation in fault zones and a study of regional joint formation around faults in limestone by Bourne and Willemsse (2001) show that a kinematic classification alone cannot explain or predict the occurrence of the structural patterns without the use of failure criteria specific to the rock type and loading conditions.

Many studies have sought simple relationships between easily measured parameters including the maximum slip across a fault, fault dimensions such as length and thickness (Hull, 1988; Evans, 1990; Bonnet et al., 2001;

Ben-Zion and Sammis, 2003), and other characteristics of the fault zone that can be used in practical applications (Knipe et al., 1998). For instance, Foxford et al. (1998) attempted to correlate the thickness of the fault zone to the distribution of throw across the Moab fault. Although our study has demonstrated that the dimensions of faults relative to their spacing or distance from the Earth’s surface influence the local state of stress, and thus the structures that form in the fault zone, our results also indicate that simple relationships between these parameters are unlikely. Rather, reliable predictions of fault zone characteristics must include an analysis of the geometric evolution of the fault and deformation mechanisms in terms of the loading history.

Impact on Fluid Flow

The relative distribution and ages of deformation bands and joints should result in varying hydrologic properties during the faulting history and along the fault. Porosity loss and pore-throat collapse in deformation bands reduces permeability (Antonellini and Aydin, 1994; Antonellini et al., 1994; Fisher and Knipe, 1998; Matthäi et al., 1998). These effects are extreme in the case of the polished slip surfaces that develop at large slip. In addition, the anastomosing geometry common to most zones of deformation bands indicate a well-connected system of low-porosity zones. Thus fault zones consisting of deformation bands reduce permeability across and within the fault zone. In contrast, opening of joints or slip across established joints, which produces dilation due to surface roughness along fracture walls (Brown, 1987), increases the permeability of joints in sandstone (Taylor et al., 1999). Slip also produces splay fractures at an angle to the sheared discontinuity, increasing secondary porosity and promoting connectivity between fractures (Dholakia et al., 1998; Flodin et al., 2001; Flodin, 2003; Myers and Aydin, 2004). The resulting fragmented rock and breccia are essentially zones of well-connected fracture porosity capable of acting as an extensive high-permeability zone facilitating fault-parallel fluid flow (Flodin et al., 2001; Jourde et al., 2002). In addition, unlike deformation bands, the permeability of joints is extremely sensitive to the effective stress state because it is correlated to the joint’s aperture.

Criteria for determining the effect of fault zones on subsurface permeability in the absence of shale often assume that fracture formation and slip generally increase permeability (e.g., Barton et al., 1995; Wiprut and Zoback, 2000). Previous studies have proposed that hydraulically conductive fractures

are generally part of the subset of fractures for which the ratio of shear traction driving slip is equal to the frictional resistance, so these fractures are critically stressed to slip (Barton et al., 1995). This hypothesis implies that actively slipping fractures maintain permeability from increased porosity (dilatancy) accompanying slip, whereas other fractures may heal or remain closed. However, along the Moab fault we have recognized two failure modes in porous sandstone, only one of which results in increased fracture porosity. Because, it is likely that the permeability structure of a fault system is a function of the aggregate properties of each structure and their connectivity in the fault zone (Caine et al., 1996; Evans et al., 1997; Flodin et al., 2001), the distinct distribution and relative timing of joints and deformation bands suggest that the fault behaved as a hybrid conduit/barrier system with conductivity varying both spatially and temporally over the faulting history.

Many diagenetic products including bitumen staining in fractures and along fault surfaces, calcite and ankerite veins (e.g., Fig. 1), calcite cement, bleaching, malachite and Liesegang banding (Foxford et al., 1996; Chan et al., 2000; Garden et al., 2001) are associated with the role of the Moab fault system as an intermittent hydrocarbon barrier and conduit. In particular, Foxford et al. (1996) reported that the most intense diagenetic alteration is localized in the Courthouse and Mill Canyon area, where we have documented joints overprinting deformation bands in relays and at intersections. These diagenetic products are far less abundant, or absent, in the remaining deformation band-dominated fault system. This finding suggests that the portion of the Moab fault overprinted by joints acted as a preferred fluid conduit whereas the deformation band-based portion of the fault did not. These results suggest that assessment of the present-day fluid-transport and sealing behavior of the Moab fault, or similar faults in the subsurface, must consider the spatial distribution of low- and high-permeability structures and their overprinting relationships resulting from fault growth by different processes.

CONCLUSIONS

The Moab fault is composed of two classes of structures where it occurs in sandstone: (1) cataclastic deformation bands and (2) brittle joints, sheared joints, and breccia. Whereas deformations bands occur everywhere in faulted sandstone, joints, sheared joints, and breccia only occur in locations of geometric complexity such as fault relays, intersections, and tips where the

slip vector indicates extension parallel to fault strike. In addition, joints overprint deformation bands, indicating that the joints are younger. These observations indicate that structural heterogeneity in the fault zone is systematically related to the geometry of the fault, but is not easily related to single parameters such as throw or fault length.

We used elastic boundary element simulations to derive the remote state of stress during faulting from kinematic data and the inferred burial depth. Simulations of relays and intersections using these remote stress boundary conditions produced less compressive σ_1 and σ_m in locations where joints were mapped. In addition, the observed orientation of joints at relays and intersections is consistent with the simulated orientation of σ_1 . We thus conclude that the transition from deformation band to joint formation was controlled by the interaction among changes in remote boundary conditions resulting from burial and exhumation, tectonic process, and fluid pressure in concert with changes in fault geometry. In addition, the systematic distribution of deformation bands and joints also suggests that the petrophysical properties of the fault zone, such as permeability, varied both along the fault and during its slip history.

ACKNOWLEDGMENTS

We thank Phil Resor for discussions and help during field work. The Rock Fracture Project at Stanford University provided both funding and a supporting environment. Our reconnaissance work on the Moab fault was initiated through a grant from ARCO thanks to Fred Dula and Russell Davies. Later this study was supported by National Science Foundation grant EAR-0229862. Frantz Maerten and David Pollard provided assistance with Poly3D. Kurt Sternloff, Michael Hudec, Haakon Fossen, associate editor John Bartley, and editor Peter Copeland reviewed the manuscript.

REFERENCES CITED

- Anderson, E.M., 1951, The dynamics of faulting and dyke formation with applications to Britain: Edinburgh, Oliver and Boyd, 206 p.
- Angelier, J., 1994, Fault slip analysis and palaeostress reconstruction, in Hancock, P.L., ed., Continental deformation: Oxford, Pergamon Press, p. 53–100.
- Antonellini, M., and Aydin, A., 1994, Effect of faulting on fluid flow in porous sandstones: Petrophysical properties: American Association of Petroleum Geologists Bulletin, v. 78, p. 355–377.
- Antonellini, M.A., Aydin, A., and Pollard, D.D., 1994, Microstructure of deformation bands in porous sandstones at Arches National Park, Utah: Journal of Structural Geology, v. 16, p. 941–959, doi: 10.1016/0191-8141(94)90077-9.
- Aydin, A., 1978, Small faults formed as deformation bands in sandstone: Pure and Applied Geophysics, v. 116, p. 913–930.
- Aydin, A., 2000, Fractures, faults, and hydrocarbon entrapment, migration and flow: Marine and Petroleum Geology, v. 17, p. 797–814, doi: 10.1016/S0264-8172(00)00020-9.

- Aydin, A., and Johnson, A.M., 1978, Development of faults as zones of deformation bands and as slip surfaces in sandstone: Pure and Applied Geophysics, v. 116, p. 931–942.
- Barton, C., Zoback, M., and Moos, D., 1995, Fluid-flow along potentially active faults in crystalline rock: Geology, v. 23, p. 683–686, doi: 10.1130/0091-7613(1995)02323.CO:2.
- Ben-Zion, Y., and Sammis, C.G., 2003, Characterization of fault zones: Pure and Applied Geophysics, v. 160, p. 677–715.
- Bieniawski, Z.T., 1984, Rock mechanics design in mining and tunneling: Rotterdam, Netherlands, A.A. Balkema, 272 p.
- Bonnet, E., Bour, O., Odling, N.E., Davy, P., Main, I., Cowie, P., and Berkowitz, B., 2001, Scaling of fracture systems in geological media: Reviews of Geophysics, v. 39, p. 347–383, doi: 10.1029/1999RG000074.
- Bott, M.H.P., 1959, The mechanics of oblique slip faulting: Geological Magazine, v. 96, p. 109–117.
- Bourne, S.J., and Willmsee, E.J.M., 2001, Elastic stress control on the pattern of tensile fracturing around a small fault network at Nash Point, UK: Journal of Structural Geology, v. 23, p. 1753–1770, doi: 10.1016/S0191-8141(01)00027-X.
- Brown, S.R., 1987, Fluid flow through rock joints: Effects of surface roughness: Journal of Geophysical Research, v. 99, p. 9373–9390.
- Bürgman, R.D., Pollard, D.D., and Martel, S.J., 1994, Slip distributions on faults: Effects of stress gradients, inelastic deformation, heterogeneous hostrock stiffness, and fault interaction: Journal of Structural Geology, v. 16, p. 1675–1690, doi: 10.1016/0191-8141(94)90134-1.
- Caine, J., Evans, J., and Forster, C., 1996, Fault zone architecture and permeability structure: Geology, v. 24, p. 1025–1028, doi: 10.1130/0091-7613(1996)02423.CO:2.
- Cartwright, J., Mansfield, C., and Trudgill, B., 1995, The growth of faults by segment linkage: Evidence from the Canyonlands grabens of S.E. Utah: Journal of Structural Geology, v. 17, p. 1319–1326, doi: 10.1016/0191-8141(95)00033-A.
- Chan, M., Parry, W.T., Bowman, J.R., 2000, Diagenetic hematite and manganese oxides and fault-related fluid flow in Jurassic sandstones, southeastern Utah: American Association of Petroleum Geologists Bulletin, v. 84, p. 1281–1310.
- Cowie, P.A., 1998, A healing-reloading feedback control on the growth rate of seismogenic faults: Journal of Structural Geology, v. 20, p. 1075–1087, doi: 10.1016/S0191-8141(98)00034-0.
- Crider, J.G., and Peacock, D.C.P., 2004, Initiation of brittle faults in the upper crust: A review of field observations: Journal of Structural Geology, v. 26, p. 691–707, doi: 10.1016/J.JSG.2003.07.007.
- Crider, J., and Pollard, D., 1998, Fault linkage: Three-dimensional mechanical interaction between echelon normal faults: Journal of Geophysical Research, v. 103, p. 24,373–24,391, doi: 10.1029/98JB01353.
- Cruikshank, K.M., and Aydin, A., 1995, Unweaving the joints in Entrada Sandstone, Arches National Park, Utah, U.S.: Journal of Structural Geology, v. 17, p. 409–421, doi: 10.1016/0191-8141(94)00061-4.
- Cruikshank, K.M., Zhao, G., and Johnson, A.M., 1991, Analysis of minor fractures associated with joints and faulted joints: Journal of Structural Geology, v. 13, p. 865–886, doi: 10.1016/0191-8141(91)90083-U.
- Davatzen, N.C., and Aydin, A., 2003, Overprinting faulting mechanisms in high porosity sandstones of SE Utah: Journal of Structural Geology, v. 25, p. 1795–1813, doi: 10.1016/S0191-8141(03)00043-9.
- Davatzen, N.C., and Aydin, A., 2004, Distribution and nature of fault architecture in a layered sandstone and shale sequence: An example from the Moab fault, Utah, in Faults, fluid flow and petroleum traps: American Association of Petroleum Geologists Memoir (in press).
- Davatzen, N.C., Aydin, A., and Eichhubl, P., 2003, Overprinting faulting mechanisms during the development of multiple fault sets in sandstone, Chimney Rock fault array, Utah, USA: Tectonophysics, v. 363, p. 1–18, doi: 10.1016/S0040-1951(02)00647-9.
- Dholakia, S.K., Aydin, A., Pollard, D.D., and Zoback, M.D., 1998, Fault-controlled hydrocarbon pathways in the Monterey Formation, California: American Association of Petroleum Geologists Bulletin, v. 82, p. 1551–1574.

- Doelling, H.H., 1982, Stratigraphic investigations of Paradox Basin structures as a means of determining the rates and geologic age of salt-induced deformation: A preliminary study: Utah Geologic and Mineral Survey Open-File Report 29, 88 p., 9 plates.
- Doelling, H.H., 1985, Geology of Arches National Park: Utah Geological and Mineral Survey Map 74, 2 p., scale 1:50,000.000
- Doelling, H.H., 1988, Geology of Salt Valley Anticline and Arches National Park, Grand County, Utah, in Doelling, H.H., Oviatt, C.G., Huntoon, P.W., eds., Salt Deformation in the Paradox Region: Salt Lake City, Utah Geological and Mineral Survey Bulletin, v. 122, p. 1–60.
- Dyer, J.R., 1983, Jointing in sandstones, Arches National Park, Utah [Ph.D. thesis]: Stanford, California, Stanford University, 275 p.
- Evans, J.P., 1990, Thickness-displacement relationships for fault zones: Journal of Structural Geology, v. 12, p. 1061–1065, doi: 10.1016/0191-8141(90)90101-4.
- Evans, J.P., Forster, C.B., and Goddard, J.V., 1997, Permeability of fault-related rocks, and implications for hydraulic structure of fault zones: Journal of Structural Geology, v. 19, p. 1393–1404, doi: 10.1016/S0191-8141(97)00057-6.
- Fisher, Q.J., and Knipe, R.J., 1998, Fault sealing processes in siliciclastic sediments, in Jones, G.A.K., Fisher, Q.J., and Knipe, R.J., eds., Faulting, fault sealing and fluid flow in hydrocarbon reservoirs: Geological Society [London] Special Publication 147, p. 117–134.
- Flodin, E.A., 2003, Structural evolution, petrophysics, and large-scale permeability of faults in sandstone, Valley of Fire, Nevada [Ph.D. thesis]: Stanford, California, Stanford University, 180 p.
- Flodin, E.A., and Aydin, A., 2004, Evolution of a strike-slip network, Valley of Fire State Park, southern Nevada: Geological Society of America Bulletin, v. 116, p. 42–59, doi: 10.1130/B25282.1.
- Flodin, E.A., Aydin, A., Durlflosky, L.J., and Yeten, B., 2001, Representation of fault zone permeability in reservoir flow models: SPE Annual Technical Conference and Exhibition, New Orleans, SPE paper 71671, p. 10.
- Foxford, K.A., Garden, I.R., Guscott, S.C., Burley, S.D., Lewis, J.J.M., Walsh, J.J., and Waterson, J., 1996, The field geology of the Moab fault, in Huffman, A.C., Lund, W.R., and Godwin, L.H., eds., Geology and resources of the Paradox Basin: Salt Lake City, Utah Geological Association Guidebook, v. 25, p. 265–283.
- Foxford, K.A., Walsh, J.J., Watterson, J., Garden, I.R., Guscott, S.C., Burley, S.D., Fisher, Q.J., and Knipe, R.J., 1998, Structure and content of the Moab fault zone, Utah, USA, and its implications for fault seal prediction, in Jones, G.A.K., Fisher, Q.J., and Knipe, R.J., eds., Faulting, fault sealing and fluid flow in hydrocarbon reservoirs: Geological Society [London] Special Publication 147, p. 87–103.
- Garden, I.R., Guscott, S.C., Burley, S.D., Foxford, K.A., Walsh, J.J., and Marshall, J., 2001, An exhumed paleo-hydrocarbon migration fairway in the Entrada Sandstone of SE Utah, USA: Geofluids, v. 1, p. 195–213, doi: 10.1046/J.1468-8123.2001.00018.X.
- Hintze, L.H., 1993, Geologic history of Utah: A field guide to Utah's rocks: Reprinted with minor revisions: Provo, Utah, Brigham Young University, 202 p.
- Hull, J., 1988, Thickness-displacement relationships for deformation zones: Journal of Structural Geology, v. 10, p. 431–435, doi: 10.1016/0191-8141(88)90020-X.
- Issen, K.A., and Rudnicki, J.W., 2000, Theory of compaction bands in porous rock: Physics and Chemistry of the Earth (A), v. 26, p. 95–100.
- Jaeger, J.C., and Cook, N.G.W., 1979, Fundamentals of rock mechanics, 3rd edition: London, Chapman and Hall, 593 p.
- Jourde, H., Flodin, E., Aydin, A., Durlflosky, L., and Wen, X., 2002, Computing permeability of fault zones in eolian sandstone from outcrop measurements: American Association of Petroleum Geologists Bulletin, v. 86, p. 1187–1200.
- Kattenhorn, S.A., and Pollard, D.D., 1999, Is lithostatic loading important for the slip behavior and evolution of normal faults in the Earth's crust?: Journal of Geophysical Research, v. 104, p. 28,879–28,898, doi: 10.1029/1999JB900297.
- Kattenhorn, S.A., Aydin, A., and Pollard, D.D., 2000, Joints at high angles to normal fault strike: An explanation using 3-D numerical models of fault-perturbed stress fields: Journal of Structural Geology, v. 22, p. 1–23, doi: 10.1016/S0191-8141(99)00130-3.
- Kim, Y.-S., Peacock, D.C.P., and Sanderson, D.J., 2004, Fault damage zones: Journal of Structural Geology, v. 26, p. 503–517, doi: 10.1016/J.JSG.2003.08.002.
- Knipe, R.J., Jones, G., Fisher, Q.J., 1998, Faulting, fault sealing and fluid flow in hydrocarbon reservoirs: An introduction, in Knipe, R.J., Jones, G., Fisher, Q.J., eds., Faulting, Fault Sealing and Fluid Flow in Hydrocarbon Reservoirs: Geological Society [London] Special Publication 147, p. vii–xxi.
- Martel, S.J., Pollard, D.D., and Segall, P., 1988, Development of simple fault zones in granitic rock, Mount Abbot quadrangle, Sierra Nevada: Journal of Geophysical Research, v. 94, p. 1451–1465.
- Matthäi, S.K., Aydin, A., Pollard, D.D., and Roberts, S., 1998, Numerical simulation of deviations from radial drawdown in a faulted sandstone reservoir with joints and zones of deformation bands, in Jones, G.A.K., Fisher, Q.J., and Knipe, R.J., eds., Faulting, fault sealing and fluid flow in hydrocarbon reservoirs: Geological Society [London] Special Publication 147, p. 157–191.
- Mavko, G., Mukerji, T., and Dvorkin, J., 1998, The rock physics handbook: Tools for seismic analysis in porous media: New York, Cambridge University Press, 329 p.
- McGrath, A.G., and Davison, I., 1995, Damage zone geometry around fault tips: Journal of Structural Geology, v. 17, p. 1011–1024, doi: 10.1016/0191-8141(94)00116-H.
- Menendez, B., Zhu, W., and Wong, T.-F., 1996, Micro-mechanics of brittle faulting and cataclastic flow in Berea Sandstone: Journal of Structural Geology, v. 18, p. 1–16, doi: 10.1016/0191-8141(95)00076-P.
- Myers, R.D., and Aydin, A., 2004, The evolution of faults formed by shearing across joint zones in sandstone: Journal of Structural Geology, v. 26, p. 947–966, doi: 10.1016/J.JSG.2003.07.008.
- Nuccio, V.F., and Condon, S.M., 1996, Burial and thermal history of the Paradox Basin, Utah and Colorado, and petroleum potential of the Middle Pennsylvanian Paradox Basin, Reston, Virginia: U.S. Geological Survey Bulletin 2000-O, p. O1–O41.
- Pevear, D.R., and Vrolijk, P.L., and Lomgstaffe, F.J., 1997, Timing of Moab fault displacement and fluid movement integrated with burial history using radiogenic and stable isotopes: Geofluids II Extended Abstracts, p. 42–45.
- Pollard, D.D., and Aydin, A., 1988, Progress in understanding jointing over the past century: Geological Society of America Bulletin, v. 100, p. 1181–1204, doi: 10.1130/0016-7606(1988)1002.3.CO:2.
- Pollard, D.D., and Segall, P., 1987, Theoretical displacements and stresses near fractures in rock: With applications to faults, joints, veins, dikes, and solution surfaces, in Atkinson, B.K., ed., Fracture mechanics of rock: London, Academic Press, p. 277–349.
- Schulz, S.E., and Evans, J.P., 2000, Mesoscopic structure of the Punchbowl fault, southern California and the geologic and geophysical structure of active strike-slip faults: Journal of Structural Geology, v. 22, p. 913–930, doi: 10.1016/S0191-8141(00)00019-5.
- Segall, P., and Pollard, D.D., 1983, Nucleation and growth of strike slip faults in granite: Journal of Geophysical Research, v. 88, p. 555–568.
- Shipton, Z.K., and Cowie, P.A., 2001, Damage zone and slip-surface evolution over μm to km scales in high-porosity Navajo sandstone, Utah: Journal of Structural Geology, v. 23, p. 1825–1844, doi: 10.1016/S0191-8141(01)00035-9.
- Shipton, Z.K., and Cowie, P.A., 2003, A conceptual model for the origin of fault damage zone structures in high-porosity sandstone: Journal of Structural Geology, v. 25, p. 333–344, doi: 10.1016/S0191-8141(02)00037-8.
- Taylor, W., Pollard, D., and Aydin, A., 1999, Fluid flow in discrete joint sets: Field observations and numerical simulations: Journal of Geophysical Research, v. 104, p. 28,983–29,006, doi: 10.1029/1999JB900179.
- Thomas, A.L., 1993, A three-dimensional, polygonal element, displacement discontinuity boundary element computer program with applications to fractures, faults, and cavities in the Earth's crust [M.S. thesis]: Stanford, California, Stanford University, 221 p.
- Underhill, R.R., and Woodcock, N.H., eds., 1987, Faulting mechanisms in high-porosity sandstones: New Red Sandstone, Arran, Scotland, in Jones, M.E., and Preston, M.F., eds., Deformation of sediments and sedimentary rocks: Geological Society [London] Special Publication 29, 91–105 p.
- Vermilye, J.M., and Scholz, C.H., 1998, The process zone: A microstructural view of fault growth: Journal of Geophysical Research, v. 103, no. B6, p. 12,223–12,237, doi: 10.1029/98JB00957.
- Willemsse, E., Pollard, D.D., and Aydin, A., 1996, Three-dimensional analyses of slip distributions on normal fault arrays with consequences for fault scaling: Journal of Structural Geology, v. 18, p. 295–309, doi: 10.1016/S0191-8141(96)80051-4.
- Willemsse, E.J.M., Peacock, D.C.P., and Aydin, A., 1997, Nucleation and growth of strike-slip faults in limestones from Somerset, U.K.: Journal of Structural Geology, v. 19, p. 1461–1477, doi: 10.1016/S0191-8141(97)00056-4.
- Wiprut, D., and Zoback, M., 2000, Fault reactivation and fluid flow along a previously dormant normal fault in the northern North Sea: Geology, v. 28, p. 595–598, doi: 10.1130/0091-7613(2000)0282.3.CO:2.

MANUSCRIPT RECEIVED BY THE SOCIETY 26 AUGUST 2003

REVISED MANUSCRIPT RECEIVED 30 MARCH 2004

MANUSCRIPT ACCEPTED 13 MAY 2004

Printed in the USA